IEEE Access
Multidisciplinary : Rapid Review : Open Access Journal

Received 10 October 2023, accepted 24 October 2023, date of publication 27 October 2023, date of current version 8 November 2023.

Digital Object Identifier 10.1109/ACCESS.2023.3328191

RESEARCH ARTICLE

NOMA With Cache-Aided Maritime D2D Communication Networks

TIEN HOA NGUYEN[1], (Member, IEEE), **JOOPYOUNG CHOI**[2], **SEONGGYOON PARK**[3], **BU-YOUNG KIM**[4], AND **WOO-SEONG SHIM**[4]

[1]School of Electrical and Electronic Engineering, Hanoi University of Science and Technology, Hanoi 100000, Vietnam
[2]Institute for Spectrum Insight Company Ltd., Cheongju 28405, South Korea
[3]Radio Engineering Department, Information & Communication School, Kongju National University, Cheonan 31080, South Korea
[4]Korea Research Institute of Ships and Ocean Engineering (KRISO), Daejeon 34103, South Korea

Corresponding author: Woo-Seong Shim (pianows@kriso.re.kr)

This research was supported by the Korea Institute of Marine Science & Technology Promotion (KIMST) funded by the Ministry of Oceans and Fisheries (1525013947).

ABSTRACT This work proposes a novel scheme of non-orthogonal multiple access (NOMA) combined with cache-enabled maritime device-to-device communication (D2D) networks, which aims to improve the performance of ship users located far from the shore and also reduce the data traffic load at the coastal base station. Taking into account the quality-of-service demands of near ship users along with the poor channel condition of far ship users, a joint beamforming design and NOMA power allocation issue is also considered. In addition, three kinds of decoding order at far ship users are also studied to comprehensively characterize the superiority of the proposed systems. Accordingly, the performance of users is then quantified in terms of outage probability and ergodic capacity, where the respective exact expressions are also evaluated in closed form. Qualitative numerical results corroborates the developed theoretical analysis and reveals that: (1) The adoption of the proposed decoding order scheme to improve the outage performance of far ship users is strongly dominated by the trade-off power setting between the coastal base station and the near ship use; and (2) The ergodic rate achieved by the proposed NOMA with cache-aided maritime full-duplex D2D communication network always outperforms those of benchmark schemes, particularly in saving at least 2.5 dB of transmitting power budget for far ship users and achieving double ergodic capacity for near ship users.

INDEX TERMS Device-to-device communications (D2D), marine vehicles, non-orthogonal multiple access (NOMA), ship-to-everythings (S2X), wireless caching.

I. INTRODUCTION

Non-orthogonal multiple access (NOMA) is a promising technique to improve the spectral efficiency and user fairness of wireless communication systems by allowing multiple users to share the same time-frequency resource with different power levels and employing successive interference cancellation (SIC) to decode the signals of different users [1], [2]. Although NOMA has been explored in variety contexts of wireless communication systems (e.g., cognitive radio [3], energy harvesting [4], visible light communication [5], reconfigurable intelligent surface [6], short-packet communication [7], etc.), such technology introduces some challenges involving high complexity, imperfect SIC, and limited coverage, which may limit its performance and practicality [8].

On the other hand, device-to-device (D2D) communication and caching techniques have recently been proposed to be integrated into NOMA systems [9], [10]. D2D communication, another key technology for 5G networks, enables users to exchange cached content directly without going through the base station, which can improve the network capacity, energy efficiency, and user experience by exploiting the spatial reuse and proximity gains [11]. Moreover, D2D

The associate editor coordinating the review of this manuscript and approving it for publication was Chan Hwang See.

communication can also support content-centric applications, such as video on demand, social networking, and mobile gaming, by leveraging the caching capability of user devices [12]. By using cache-aided D2D communication, users can exchange their cached content with each other via a direct link, which can further enhance the data rates and offload the base stations [13].

Maritime communication has recently become an important service for various ship-to-everythings (S2X) including S2S (Ship to Ship), S2I (Ship to Infra), S2N (Ship to Network), S2A (Ship to Air), S2P (Ship to People) applications, such as navigation, safety, surveillance, and environmental monitoring [14]. Research on maritime communication has recently gained significant attention. For examples, KRISO (Korea's Research Institute of Ships and Ocean Engineering) has conducted a review of suitable candidate radio spectrum bands for S2S communication from 2021. As a result, TVWS (TV White Space) using the UHF band, which is a representative wireless device using unlicensed bands, and Wi-Fi using the 2.4GHz and 5GHz bands were selected as candidate frequency bands for S2S communication, and in the second half of 2023, KRISO will be conduct real-world environmental tests [15]. Based on the feasibility of S2S communication in unlicensed bands in 2023, it plans to continuously explore various additional candidate radio spectrum bands for S2X communication. In the future, since the use of various radio spectrum bands for S2X communication is planned, it is anticipated that radio interference between homogeneous wireless networks may increase and QoS reduction may occur in using S2X communication.

However, different from conventional terrestrial communication systems, maritime communications are limited in their ability to provide reliable and ubiquitous coverage for vast ocean areas due to the limited transmission range and the harsh propagation environment, such as dynamic topology, sparse deployment, and severe fading [16], [17]. Especially, it is a challenge to deal with maritime devices with limited storage and ability in maritime communication networks. In this context, the use of caching, which stores popular or reusable content on the user's devices in advance, can reduce the data traffic and latency of content delivery. To determine content storage, update cached content, and coordinate updates among devices, some cache optimization strategies has been considered in the literature, such as applying shipping lane information at base stations to predict future user associations and optimize caching placement and transmission [18], using cooperative caching schemes to achieve content popularity and freshness [19], and exploiting device mobility to optimize task offloading and caching decisions for optimizing task offloading and caching decisions to edge servers [20]. In particular, the realization of NOMA with cache-aided D2D communication becomes a promising solution to provide seamless and flexible coverage for the maritime domain, where users on ships or islands have limited access to terrestrial networks and often request similar content [21]. In this scenario, the exploitation of NOMA plays an important role in simultaneously serving multiple users in the same cell with different channel conditions and quality-of-service (QoS) requirements [22], [23], while cache-aided D2D communication can be used to deliver cached content among nearby users with common interests. Nevertheless, to the best authors' knowledge, there is no research on the performance of NOMA with cache-aided maritime D2D communication networks in the literature.

From the aforementioned above, this work, therefore, proposes a NOMA based D2D communication method for S2S communication in unlicensed bands. The proposed approach involves cache-aided maritime D2D communication networks, employing full-duplex D2D communications for near ship users to transfer cached contents to far users. At the coastal base station, the NOMA paradigm is utilized to simultaneously serve near ship users and deliver requested contents unavailable at far ship users. To enhance the performance of far ship users and maintain QoS for near ship users, the study explores joint beamforming and NOMA power allocation design. Three distinct decoding order schemes for far ship users are quantified to optimize their performance: Case I, the signal produced by D2D communications is set to be the lowest priority; Case II, the signal produced by D2D communications is set to be higher than its signal transmitted by the coastal base station but lower than near ship user's signal; and Case III: the signal produced by D2D communications has the highest priority. In a nutshell, the key contributions of this paper include

1) This work proposes NOMA with cache-aided maritime D2D communication networks, where ship users anchored far from the coastal base station can exchange cached content via ship near users' full-duplex D2D communications and receive enhanced signal quality over direct beamforming transmissions.
2) Capitalizing on the information transmitted by the coastal base station and D2D communications, three decoding order schemes for far ship users are considered and investigated.
3) Aiming to capture the main system characteristics, the performance of users in terms of outage probability and ergodic rate has been explored and derived in closed-form expressions, which are then particularly useful to observe and deduce the performance trend in different power-setting scenarios.
4) Numerical results verify the correctness of the derived theoretical analysis and shows that:
   - When the transmit power of the base station is smaller than that of the D2D transmission power, the decoding order corresponding to case III is recommended to reduce far ship users' outage performance. Otherwise, the decoding order associated with case I should be applied.
   - The adoption of more antenna transmission only makes sense to the performance of far ship users

when the transmit power of the base station is comparatively higher than that of the D2D transmission power and the decoding order involved in case I is jointly considered.
- When the transmit power of the base station is comparatively smaller than that of the D2D transmission power, optimizing the PA policy for improving far-ship users' performance is only possible with the adoption of the decoding order involving case III, otherwise, the case II is the best as an increase in PA coefficient of near-ship users can simultaneously improve both users.
- The proposed system with three decoding order schemes can achieve better EC enhancement than those of half-duplex D2D systems as well as conventional cooperative NOMA ones in [16].
- When the increased number of antenna transmissions and transmit power of the base station are jointly considered, the performance of far ship users can be significantly enhanced with the robustness of beamforming design.
- There is an EC trade-off when allocating power budget between users.

The rest of the paper is outlined as follows: Section II describes the system model and information transmission with three decoding order schemes. Section III analyzes the two performance metrics, namely outage probability and ergodic capacity, and derives the respective closed-form expressions. Section IV corroborates the theoretical analysis through simulation results, as well as points out new observations brought by each proposed decoding order, and finally Section V concludes the paper.

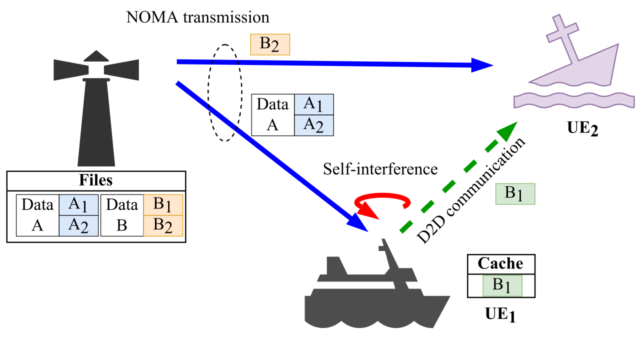

FIGURE 1. Systems model with D2D communication.

II. SYSTEM MODEL

A. SYSTEM MODEL DESCRIPTION

Consider maritime-based NOMA networks in Fig. 1 including one coastal base station (S) having K antennas and two destination nodes (ship users, denoted by U_1 and U_2), where single-antenna U_2 is anchored far from the S while U_1 having couple antenna locates nearby from shore. The distance from U_1 to U_2 is smaller than that of from S to U_2. Both ship users are served with separate data information U_1 and U_2 requesting for A and B files, respectively, and each file has two sub-files, indexed by 1 and 2. In a dynamic maritime environment, user preferences and content popularity can vary and this poses a challenge in designing efficient content prefetching and delivery mechanisms. To solve this problem, some possible solutions can be considered by using mobility prediction and joint user prefetching to optimize the content caching strategy [24], or web communities identification and outsourcing to improve the content distribution network performance [25]. Note that all of the issues related to identifying and distributing caching content are beyond the scope of this work. It is assumed that a portion of U_2' request B_1 is stored in the cache of U_1, which facilitates the establishment of D2D communication from U_1 to U_2. Accordingly, in order to improve the spectral resources and serve both users at the same time, NOMA is considered at the BS to send a superposed message composed of content A and sub-files B_2 while full-duplex D2D communication is exploited at U_1 to forward the cached sub-file B_1 to U_2.

In practical scenarios, maritime networks typically serve a huge number of users; however, due to device mobility and changing topologies. This can result in different interference patterns, triggering the need for efficient interference management strategies to ensure that users experience acceptable signal quality. In this context, the exploitation of hybrid NOMA transmission mode is necessary to further improve spectrum utilization as well as eliminate the impact of interference [26]. In particular, NOMA users are grouped into multiple clusters, each cluster has two users (a basic form has been standardized in 3GPP) and time-division or orthogonal frequency transmissions are scheduled to serve the communication of each group. In this way, the issue of cell and intra-cell interference can be reduced. Accordingly, the adoption of our proposed model is still applicable as it is a basic form of the NOMA cluster.

B. INFORMATION TRANSMISSION

Let $[\mathbf{h}_1]_k$, $[\mathbf{h}_2]_k$, h_{12}, and h_{11} be the non-identical and independent Rayleigh fading channel coefficients [16] from the k-th antennas of S to U_1, from the k-th antennas of BS to U_2, from U_1 to U_2 and from U_1 to itself, respectively, with $k = 1, 2, \ldots, K$. Accordingly, these channels distribution can be mathematically modeled as $[\mathbf{h}_1]_k \sim \mathcal{CN}(0, \lambda_1)$, $[\mathbf{h}_2]_k \sim \mathcal{CN}(0, \lambda_2)$, $h_{12} \sim \mathcal{CN}(0, \lambda_{12})$, and $h_{11} \sim \mathcal{CN}(0, \lambda_{11})$, where $\{\lambda_1, \lambda_2, \lambda_{12}$, and λ_{11} are the scale parameters. The received signals at ship users can be expressed by

$$y_{U_1} = x_{NOMA}\mathbf{h}_1\mathbf{w} + h_{11}\sqrt{P_{U_1}}x_{B_1} + n_1, \quad (1)$$

$$y_{U_2} = x_{NOMA}\mathbf{h}_2\mathbf{w} + h_{12}\sqrt{P_{U_1}}x_{B_1} + n_2, \quad (2)$$

where $x_{NOMA} = \sqrt{\delta_1 P_S}x_A + \sqrt{\delta_2 P_S}x_{B_2}$ is the NOMA message produced by the BS with the transmission power available P_S and the power allocated to U_1's message of δ_1 ($\delta_1 + \delta_2 = 1$), x_{B_1} is the transmitted message from U_1, $\mathbf{w}$ is the matched filter vector, P_{U_1} is the power allocated for D2D transmissions, and $\{n_1, n_2\}$ are the Gaussian noise with zero-mean and variance σ.

As seen from the expressions above, users receive three distinct messages, and their performance is determined by different SIC decoding orders. To ensure systematic decoding of messages while also meeting the quality service constrained by U_1 and enhancing U_2' performance, the NOMA power allocation (PA) is set so that the following decoding order $x_A \rightarrow x_{B_2}$ holds, i.e., $\delta_1 \geq \delta_2$, and the beamforming vector $\mathbf{w}$ is established so as $\mathbf{w} = \mathbf{h}_2^H/\|\mathbf{h}_2\|$. Thus, U_1 only needs to recover the requested content A by treating the signal of sub-file B_2 and the self-interference from the signal of sub-file B_1 as noise. Denote by $\|\hat{\mathbf{h}}_1\|^2 \triangleq \|\mathbf{h}_1\mathbf{w}\|^2$, the signal-to-interference-plus-noise ratio (SINR) received by U_1 to decode x_A is given by

$$\gamma_{U_1 \rightarrow x_A} = \frac{\delta_1 P_S \|\hat{\mathbf{h}}_1\|^2}{\delta_2 P_S \|\hat{\mathbf{h}}_1\|^2 + P_{U_1}|h_{11}|^2 + \sigma}. \quad (3)$$

At U_2, following the SIC mechanism, the decoding order is set so that the message with the highest priority QoS would be first decoded subject to the predefined decoding order of $x_A \rightarrow x_{B_2}$. Therewith, the decoding order can be distinguished by

- **Case I**: The decoding order at U_2 is set to be the information in file A from the source node, then information in file B_2, and finally information in sub-file B_1 from the near ship user achieved by full-duplex-assisted D2D communication. The received SINRs to decode x_A, x_{B_2}, and x_{B_1} can be, respectively, expressed as

$$\gamma^{I}_{U_2 \rightarrow x_A} = \frac{\delta_1 P_S \|\mathbf{h}_2\|^2}{\delta_2 P_S \|\mathbf{h}_2\|^2 + P_{U_1}|h_{12}|^2 + \sigma}, \quad (4)$$

$$\gamma^{I}_{U_2 \rightarrow x_{B_2}} = \frac{\delta_2 P_S \|\mathbf{h}_2\|^2}{P_{U_1}|h_{12}|^2 + \sigma}, \quad (5)$$

$$\gamma^{I}_{U_2 \rightarrow x_{B_1}} = \frac{P_{U_1}|h_{12}|^2}{\sigma}. \quad (6)$$

- **Case II**: The decoding order at U_2 is set such that the information in file A from the source node is first decoded, then the information in sub-file B_1, and finally information in file B_2. Then after cancellation, file A can be decoded the same SINR in (4), i.e., $\gamma^{II}_{U_2 \rightarrow x_A} = \gamma^{I}_{U_2 \rightarrow x_A}$, the SINRs associated with the decoding of sub-files B_1 and B_2 are respectively given by

$$\gamma^{II}_{U_2 \rightarrow x_{B_1}} = \frac{P_{U_1}|h_{12}|^2}{\delta_2 P_S \|\mathbf{h}_2\|^2 + \sigma}, \quad (7)$$

$$\gamma^{II}_{U_2 \rightarrow x_{B_2}} = \frac{\delta_2 P_S \|\mathbf{h}_2\|^2}{\sigma}. \quad (8)$$

- **Case III**: The decoding order at U_2 is first determined by the information in sub-file B_1, then information in file A, and finally information in file B_2. The received SINRs associated with x_{B_1} and x_A can be expressed, respectively, as

$$\gamma^{III}_{U_2 \rightarrow x_{B_1}} = \frac{P_{U_1}|h_{12}|^2}{P_S \|\mathbf{h}_2\|^2 + \sigma}, \quad (9)$$

$$\gamma^{III}_{U_2 \rightarrow x_A} = \frac{\delta_1 P_S \|\mathbf{h}_2\|^2}{\delta_2 P_S \|\mathbf{h}_2\|^2 + \sigma}. \quad (10)$$

Meanwhile, the SINR to decode x_{B_2} is given in (8).

From the three above cases, it is clear that in case I, the decoding order enables U_1 to transmit a lower transmission power without exhausting its power budget. Meanwhile, the decoding order in case II gives U_2 a chance to boost the signal power strength of file B_2 by leveraging the beamforming design and (or) resource PA at the source node. Unlike case II, the decoding order in case III requires U_1 to pay some interest from its power budget to quickly respond to U_2's services (i.e., file B_1), in return, the source node gives U_1 a chance to be served with a higher power budget. However, it should be noted that exploiting full-duplex communication at U_1 to convey files B_1 to U_2 will result in inevitable self-interference from the broadcasting signal to the sensitive receiver. In order to realize such caching-aided D2D communication while ensuring the performance of U_1 for practical scenarios, U_1 must be equipped with properly self-interference cancellation approaches, including antenna isolation/polarization, or analog, and digital domains, in conjunction with reasonable circuits and algorithms [27]. Along with that, as U_2 receives two different signals, one from the base station and the other via U_1, levering the SIC mechanism to separate such information from each other might increase the outage performance at U_2. In return, U_2 can achieve a higher ergodic capacity. Therefore, depending on specific applications in real scenarios, there is a need to select the right decoding order scheme in conjunction with proper resource allocation to achieve a lower outage performance while reaching the valid EC. More details of each scheme shall soon be delivered in the following numerical results and discussions.

III. PERFORMANCE ANALYSIS

This work aims to evaluate the performance of the considered system by focusing on two performance metric. First, the outage probability (OP) is a good candidate, as it lets us know how much probability there is that sending data information to the intended destination can be successful. Second, the ergodic capacity (EC) rate, another appealing metric, reveals to us how much the maximum spectral efficiency that the system can be achieved. Based on the SINR formula associated with three cases in Sec. II, the relevant closed-form expressions for OP and EC are derived, which will therefore help to highlight some important observations in configuring the power budget as well as managing the interference levels.

A. OUTAGE PROBABILITY ANALYSIS

This subsection will evaluate the OP expression of three cases before quantifying the impact of system parameters on each case. In definition, the OP is defined as the probability at which the SINR received by users falls below a predefined threshold $\bar{\gamma}_{\rm C} = 2^{R_{\rm C}} - 1$ for the indented information $\rm C \in \{A, B_1, B_2\}$, where $R_{\rm C}$ is the target transmission data rate.

1) OUTAGE PROBABILITY OF U_1

According to the definition of OP above, the OP for $\rm U_1$ based on (3) is given by

$$P_{\rm U_1}^{\rm out} = \Pr\left[\gamma_{\rm U_1 \to x_A} \le \bar{\gamma}_{\rm A}\right] = \Pr\left[\frac{\delta_1 - \delta_2\bar{\gamma}_{\rm A}}{P_{\rm U_1}|h_{11}|^2 + \sigma} \le \frac{\bar{\gamma}_{\rm A}}{P_{\rm S}\|\hat{\mathbf{h}}_1\|^2}\right]. \quad (11)$$

As observed, when $\delta_1 - \delta_2\bar{\gamma}_{\rm A} < 0$, the above always holds, which means $P_{\rm U_1}^{\rm out} = 1$. Otherwise, the above expression can be rewritten as

$$\begin{aligned} P_{\rm U_1}^{\rm out} &= \Pr\left[\|\hat{\mathbf{h}}_1\|^2 \le \bar{\gamma}_{\rm A}\frac{P_{\rm U_1}|h_{11}|^2 + \sigma}{P_{\rm S}(\delta_1 - \delta_2\bar{\gamma}_{\rm A})}\right] \\ &= \int_0^\infty F_{\|\hat{\mathbf{h}}_1\|^2}\left(\frac{\bar{\gamma}_{\rm A}(P_{\rm U_1}x + \sigma)}{P_{\rm S}(\delta_1 - \delta_2\bar{\gamma}_{\rm A})}\right) f_{|h_{11}|^2}(x)dx \\ &= 1 - \frac{1}{\lambda_{11}}\exp\left(-\frac{\bar{\gamma}_{\rm A}\sigma}{\lambda_1 P_{\rm S}(\delta_1 - \delta_2\bar{\gamma}_{\rm A})}\right) \\ &\quad \times \int_0^\infty \exp\left(-\left[\frac{\bar{\gamma}_{\rm A}P_{\rm U_1}}{\lambda_1 P_{\rm S}(\delta_1 - \delta_2\bar{\gamma}_{\rm A})} + \frac{1}{\lambda_{11}}\right]x\right)dx, \end{aligned} \quad (12)$$

where $F_{\|\hat{\mathbf{h}}_1\|^2}(z) = 1 - \exp(-z/\lambda_1)$ [7] and $f_{|h_{11}|^2}(x) = \exp(-x/\lambda_{11})/\lambda_{11}$. Solving the above integral, the following lemma is obtained.

Lemma 1. *Exact closed-form expressions for the OP of U_1 can be expressed as*

$$P_{U_1}^{out} = \begin{cases} 1, & \delta_1 < \delta_2\bar{\gamma}_A, \\ 1 - \dfrac{\exp\left(-\frac{\bar{\gamma}_A\sigma}{\lambda_1 P_S(\delta_1 - \delta_2\bar{\gamma}_A)}\right)}{\lambda_{11}\left(\frac{\bar{\gamma}_A P_{U_1}}{\lambda_1 P_S(\delta_1 - \delta_2\bar{\gamma}_A)} + \frac{1}{\lambda_{11}}\right)}, & \delta_1 > \delta_2\bar{\gamma}_A. \end{cases} \quad (13)$$

The above lemma reveals some important observations under conditions $\delta_1 > \delta_2\bar{\gamma}_{\rm A}$ as follows:

- When $P_{\rm S} \gg P_{\rm U_1}$, by considering $P_{\rm S} \to \infty$ and fixed $P_{\rm U_1}$, one can infer that $P_{\rm U_1}^{\rm out} \to 0$. Accordingly, $\rm U_2$ has a chance to improve its performance with the raised connectivity from $\rm U_1$.
- When $P_{\rm S} \ll P_{\rm U_1}$, by considering $P_{\rm U_1} \to \infty$ and fixed $P_{\rm S}$,it is clear that $P_{\rm U_1}^{\rm out} \to 1$ since the exponential function converges to zero. Thus, $\rm U_1$ is not recommended to realize D2D communications.
- When $(P_{\rm S} \approx P_{\rm U_1}) \to \infty$, $P_{\rm U_1}^{\rm out} \to 1 - \lambda_1(\delta_1 - \delta_2\bar{\gamma}_{\rm A})/[\lambda_{11}\bar{\gamma}_{\rm A} + \lambda_1(\delta_1 - \delta_2\bar{\gamma}_{\rm A})]$. Obviously, there is an error outage floor at $\rm U_1$.

2) OUTAGE PROBABILITY OF U_2

At $\rm U_2$, the decoding order is distinguished by three cases, which can be one-by-one evaluated as follows.

For case I, from the OP definition, the OP of $\rm U_2$ can be obtained by using the complementary probability when evaluating the SINRs received in (4), (5), and (6), as follows:

$$\begin{aligned} P_{\rm U_2,I}^{\rm out} &= 1 - \Pr[\gamma_{\rm U_2 \to x_C}^{\rm I} > \bar{\gamma}_{\rm C}, \forall {\rm C} = {\rm A, B_1, B_2}] \\ &= 1 - \Pr\Bigg[\|\mathbf{h}_2\|^2 > \bar{\gamma}_{\rm A}\frac{P_{\rm U_1}|h_{12}|^2 + \sigma}{P_{\rm S}(\delta_1 - \delta_2\bar{\gamma}_{\rm A})}, \|\mathbf{h}_2\|^2 > \bar{\gamma}_{\rm B_2} \\ &\qquad \frac{P_{\rm U_1}|h_{12}|^2 + \sigma}{\delta_2 P_{\rm S}}, |h_{12}|^2 > \bar{\gamma}_{\rm B_1}\frac{\sigma}{P_{\rm U_1}}\Bigg] \\ &= 1 - \Pr\left[\|\mathbf{h}_2\|^2 > \frac{P_{\rm U_1}|h_{12}|^2 + \sigma}{\Xi_1 P_{\rm S}}, |h_{12}|^2 > \frac{\bar{\gamma}_{\rm B_1}\sigma}{P_{\rm U_1}}\right] \\ &= 1 - \int_{\frac{\bar{\gamma}_{\rm B_1}\sigma}{P_{\rm U_1}}}^\infty \left[1 - F_{\|\mathbf{h}_2\|^2}\left(\frac{P_{\rm U_1}x + \sigma}{\Xi_1 P_{\rm S}}\right)\right] f_{|h_{12}|^2}(x)dx, \end{aligned} \quad (14)$$

where $\Xi_1 = \min\{(\delta_1 - \delta_2\bar{\gamma}_{\rm A})/\bar{\gamma}_{\rm A}, \delta_2/\bar{\gamma}_{\rm B_2}\}$ and $F_{\|\mathbf{h}_2\|^2}(z) = 1 - \exp(-z/\lambda_2)\sum_{k=0}^{K-1}(z/\lambda_2)^k/k!$ [7] and $f_{|h_{12}|^2}(x) = \exp(-x/\lambda_{12})/\lambda_{12}$. Solving the above using [28, Eq. (3.351.2)], the following lemma is attained.

Lemma 2. *Exact closed-form expressions for the OP of U_2 with case I is written as*

$$P_{U_2,I}^{out} = 1 - \sum_{k=0}^{K-1}\frac{\exp\left(-\sigma/[\lambda_2\Xi_1 P_S]\right)}{k!\lambda_{12}(\lambda_2\Xi_1 P_S)^k}\sum_{l=0}^{k}\binom{k}{l}P_{U_1}^l(\sigma)^{k-l} \times \frac{\Gamma\left(l+1, \left(\frac{P_{U_1}}{\lambda_2\Xi_1 P_S} + \frac{1}{\lambda_{12}}\right)\frac{\bar{\gamma}_{B_1}\sigma}{P_{U_1}}\right)}{\left(\frac{P_{U_1}}{\lambda_2\Xi_1 P_S} + \frac{1}{\lambda_{12}}\right)^{l+1}}. \quad (15)$$

The above lemma reveals some observations as follows:

- When $P_{\rm S} \gg P_{\rm U_1}$, by considering $P_{\rm S} \to \infty$ and fixed $P_{\rm U_1}$, the OP of $\rm U_2$ is then simplified bye considering $F_{\|\mathbf{h}_2\|^2}(\cdot) \simeq 0$, yielding
$$P_{\rm U_2,I}^{\rm out} \approx 1 - \int_{\frac{\bar{\gamma}_{\rm B_1}\sigma}{P_{\rm U_1}}}^\infty f_{|h_{12}|^2}(x)dx = 1 - \exp\left(-\frac{\bar{\gamma}_{\rm B_1}\sigma}{P_{\rm U_1}\lambda_{12}}\right).$$
It is found that the OP of $\rm U_2$ can be improved by either increasing $P_{\rm U_1}$ or decreasing $\bar{\gamma}_{\rm B_1}$.
- When $P_{\rm S} \ll P_{\rm U_1}$, by considering $P_{\rm U_1} \to \infty$ and fixed $P_{\rm S}$, the OP of $\rm U_2$ is given by $P_{\rm U_2,I}^{\rm out} \to 1$.
- When $(P_{\rm S} \approx P_{\rm U_1}) \to \infty$, the OP of $\rm U_2$ converges to the ceiling which is determined by
$$P_{\rm U_2,I}^{\rm out} \approx 1 - \sum_{k=0}^{K-1}\frac{\lambda_2\Xi_1}{(\lambda_{12} + \lambda_2\Xi_1)^{k+1}}.$$
For given the estimated variances λ_{12} and λ_2, one can handle the number of antenna setting K and the PA

coefficients and the threshold associated with Ξ_1 to produce the expected OP at U_2.

Likewise, the OP of U_2 for case II can be obtained by evaluating the SINRs received in (4), (7), and (8) as follows:

$$\begin{aligned} P^{\text{out}}_{\text{U}_2,\text{II}} &= 1 - \Pr[\gamma^{\text{II}}_{\text{U}_2\to x_\text{C}} > \bar{\gamma}_\text{C}, \forall \text{C} = \text{A}, \text{B}_1, \text{B}_2] \\ &= 1 - \Pr\Bigg[|h_{12}|^2 > \frac{\|\mathbf{h}_2\|^2\delta_2 P_\text{S} + \sigma}{P_{\text{U}_1}/\bar{\gamma}_{\text{B}_1}}, \|\mathbf{h}_2\|^2 > \frac{\bar{\gamma}_{\text{B}_2}\sigma}{\delta_2 P_\text{S}} \\ &, \|\mathbf{h}_2\|^2 > \frac{\bar{\gamma}_\text{A}\sigma/P_\text{S}}{\delta_1 - \delta_2\bar{\gamma}_\text{A}}, |h_{12}|^2 < \frac{\|\mathbf{h}_2\|^2 P_\text{S}(\delta_1 - \delta_2\bar{\gamma}_\text{A}) - \bar{\gamma}_\text{A}\sigma}{\bar{\gamma}_\text{A} P_{\text{U}_1}}\Bigg] \\ &= 1 - \int_{\frac{\Xi_2}{P_\text{S}}}^{\infty} \Bigg[F_{|h_{12}|^2}\left(\frac{P_\text{S}(\delta_1 - \delta_2\bar{\gamma}_\text{A})x - \bar{\gamma}_\text{A}\sigma}{\bar{\gamma}_\text{A}P_{\text{U}_1}}\right) \\ &\quad - F_{|h_{12}|^2}\left(\frac{\delta_2 P_\text{S} x + \sigma}{P_{\text{U}_1}/\bar{\gamma}_{\text{B}_1}}\right)\Bigg] f_{\|\mathbf{h}_2\|^2}(x)dx, \end{aligned} \tag{16}$$

where $\Xi_2 = \max\{\bar{\gamma}_{\text{B}_2}\sigma/\delta_2, \bar{\gamma}_\text{A}\sigma/(\delta_1 - \delta_2\bar{\gamma}_\text{A})\}$, $f_{\|\mathbf{h}_2\|^2}(x) = \partial F_{\|\mathbf{h}_2\|^2}(x)/\partial x = x^{K-1}\exp(-x/\lambda_2)/[\Gamma(K)\lambda_2^K]$, and $F_{|h_{12}|^2}(z) = \int_0^z f_{|h_{12}|^2}(x)dx = 1 - \exp(-z/\lambda_{12})$. Substituting $f_{\|\mathbf{h}_2\|^2}(x)$ and $F_{|h_{12}|^2}(z)$ into (16) and performing [28, Eq. (3.381.3)], the following lemma is concluded.

Lemma 3. *Exact closed-form expressions for the OP of U_2 with case II is written as*

$$\begin{aligned} P^{out}_{U_2,II} = 1 - \frac{1/\lambda_2^K}{\Gamma(K)}\Bigg[&\frac{\Gamma\left(K, \frac{\delta_2\Xi_2\bar{\gamma}_{B_1}}{\lambda_{12}P_{U_1}} + \frac{\Xi_2}{\lambda_2 P_S}\right)}{\exp\left(\frac{\bar{\gamma}_{B_1}\sigma}{\lambda_{12}P_{U_1}}\right)\left(\frac{\delta_2 P_S\bar{\gamma}_{B_1}}{\lambda_{12}P_{U_1}} + \frac{1}{\lambda_2}\right)^K} \\ &- \frac{\Gamma\left(K, \frac{\Xi_2(\delta_1 - \delta_2\bar{\gamma}_A)}{\lambda_{12}\bar{\gamma}_A P_{U_1}} + \frac{\Xi_2}{\lambda_2 P_S}\right)}{\exp\left(-\frac{\sigma}{\lambda_{12}P_{U_1}}\right)\left(\frac{P_S(\delta_1 - \delta_2\bar{\gamma}_A)}{\lambda_{12}\bar{\gamma}_A P_{U_1}} + \frac{1}{\lambda_2}\right)^K}\Bigg]. \end{aligned} \tag{17}$$

The above lemma reveals us some key points as

- When $P_\text{S} \gg P_{\text{U}_1}$, the OP of U_2 becomes 1.
- When $P_\text{S} \ll P_{\text{U}_1}$, the OP of U_2 converges to 1.
- When $(P_\text{S} \approx P_{\text{U}_1}) \to 0$, the OP of U_2 saturates

$$\begin{aligned} P^{\text{out}}_{\text{U}_2,\text{II}} &\approx 1 + \left(\frac{\lambda_{12}\bar{\gamma}_\text{A}}{\lambda_{12}\bar{\gamma}_\text{A} + \lambda_2(\delta_1 - \delta_2\bar{\gamma}_{\text{B}_1})}\right)^K \\ &\quad - \left(\frac{\lambda_{12}}{\lambda_{12} + \delta_2\lambda_2\bar{\gamma}_{\text{B}_1}}\right)^K. \end{aligned}$$

Regarding case III, the OP of U_2 evaluated by the SINRs received in (9), (10), and (8) as follows:

$$\begin{aligned} P^{\text{out}}_{\text{U}_2,\text{III}} &= 1 - \Pr\left[\gamma^{\text{III}}_{\text{U}_2\to x_\text{C}} > \bar{\gamma}_\text{C}, \forall \text{C} = \text{A}, \text{B}_1, \text{B}_2\right] \\ &= 1 - \Pr\left[|h_{12}|^2 > \bar{\gamma}_{\text{B}_1}\frac{P_\text{S}\|\mathbf{h}_2\|^2 + \sigma}{P_{\text{U}_1}}, \|\mathbf{h}_2\|^2 > \frac{\Xi_2}{P_\text{S}}\right] \\ &= 1 - \int_{\frac{\Xi_2}{P_\text{S}}}^{\infty}\left[1 - F_{|h_{12}|^2}\left(\frac{P_\text{S}x + \sigma}{P_{\text{U}_1}/\bar{\gamma}_{\text{B}_1}}\right)\right] f_{\|\mathbf{h}_2\|^2}(x)dx. \end{aligned} \tag{18}$$

Replacing $F_{|h_{12}|^2}(z)$ and $f_{\|\mathbf{h}_2\|^2}(x)$ into (18) and then using [28, Eq. (3.381.3)], the following lemma is derived.

Lemma 4. *Exact closed-form expressions for the OP of U_2 with case III can be computed as*

$$P^{out}_{U_2,III} = 1 - \frac{\Gamma\left(K, \frac{\Xi_2\bar{\gamma}_{B_1}}{\lambda_{12}P_{U_1}} + \frac{\Xi_2}{\lambda_2 P_S}\right)/\lambda_2^K}{\Gamma(K)\exp\left(\frac{\bar{\gamma}_{B_1}\sigma}{\lambda_{12}P_{U_1}}\right)\left(\frac{\bar{\gamma}_{B_1}P_S}{\lambda_{12}P_{U_1}} + \frac{1}{\lambda_2}\right)^K}. \tag{19}$$

Based on the above lemma, one can deduce that

- When $P_\text{S} \gg P_{\text{U}_1}$, the OP of U_2 becomes 1.
- When $P_\text{S} \ll P_{\text{U}_1}$, the OP of U_2 downs to $P^{\text{out}}_{\text{U}_2,\text{III}} \approx 1 - \Gamma(K, \Xi_2/[\lambda_2 P_\text{S}])/\Gamma(K)$. Improving OP of U_2 can be tackled by increasing K or P_S.
- When $(P_\text{S} \approx P_{\text{U}_1}) \to 0$, the OP of U_2 converges to $P^{\text{out}}_{\text{U}_2,\text{III}} \approx 1 - (\lambda_{12}/[\lambda_{12} + \lambda_2\bar{\gamma}_{\text{B}_1}])^K$. This means that the changes in the setting of $\bar{\gamma}_{\text{B}_1}$ and K can directly affect the OP trend of U_2.

B. ERGODIC CAPACITY ANALYSIS

This subsection will evaluate the EC expression of users under three cases. The EC of transmitted signal over the aid interference is evaluated by

$$\begin{aligned} \text{EC} &= \text{E}\{\log_2(1 + \gamma^j_{\text{U}_i\to x_\text{C}})\} = \int_0^\infty \log_2(1+x) f_{\gamma^j_{\text{U}_i\to x_\text{C}}}(x)dx \\ &= \int_0^\infty \frac{1 - F_{\gamma^j_{\text{U}_i\to x_\text{C}}}(x)}{\ln(2)(1+x)}dx, \end{aligned} \tag{20}$$

where $i \in \{1, 2\}$ and $j \in \{\text{I,II,III}\}$.

1) ERGODIC CAPACITY OF U_1

From the EC definition, the EC of U_1 can be evaluated by

$$\text{EC}_{\text{U}_1} = \int_0^\infty \frac{1 - F_{\gamma_{\text{U}_1\to x_\text{A}}}(x)}{\ln(2)(1+x)}dx, \tag{21}$$

where $F_{\gamma_{\text{U}_1\to x_\text{A}}}(x)$ is evaluated by $\Pr[\gamma_{\text{U}_1\to x_\text{A}} < x]$ (analogue to the derivation of (12)), yielding

$$F_{\gamma_{\text{U}_1\to x_\text{A}}}(x) = 1 - \frac{\exp\left(-\frac{x\sigma/[\lambda_1 P_\text{S}]}{(\delta_1 - \delta_2 x)}\right)}{\left(\frac{x\lambda_{11}P_{\text{U}_1}}{\lambda_1 P_\text{S}(\delta_1 - \delta_2 x)} + 1\right)}, 0 < x < \frac{\delta_1}{\delta_2}. \tag{22}$$

By inserting the above result into (21) and making the change variable of $y = x/[\delta_1 - \delta_2 x]$, the EC of U_1 can be derived as

$$\begin{aligned} \text{EC}_{\text{U}_1} &= \frac{\lambda_1 P_\text{S}\delta_1}{\ln(2)\delta_2\lambda_{11}P_{\text{U}_1}} \int_0^\infty \frac{\exp\left(-\frac{\sigma y}{\lambda_1 P_\text{S}}\right)dy}{(1+y)\left(y + \frac{\lambda_1 P_\text{S}}{\lambda_{11}P_{\text{U}_1}}\right)\left(y + \frac{1}{\delta_2}\right)} \\ &= \frac{\lambda_1 P_\text{S}\delta_1}{\ln(2)\delta_2\lambda_{11}P_{\text{U}_1}} \int_0^\infty \left[\frac{\alpha_1}{y+1} + \frac{\alpha_2}{y + \frac{\lambda_1 P_\text{S}}{\lambda_{11}P_{\text{U}_1}}} + \frac{\alpha_3}{y + \frac{1}{\delta_2}}\right] \\ &\quad \times \exp\left(-\frac{\sigma y}{\lambda_1 P_\text{S}}\right)dy, \end{aligned} \tag{23}$$

where the second step utilizes partial fraction methods by letting $\alpha_1 = 1/[(\frac{\lambda_1 P_S}{\lambda_{11} P_{U_1}} - 1)(\frac{1}{\delta_2} - 1)]$, $\alpha_2 = 1/[(1 - \frac{\lambda_1 P_S}{\lambda_{11} P_{U_1}})(\frac{1}{\delta_2} - \frac{\lambda_1 P_S}{\lambda_{11} P_{U_1}})]$, and $\alpha_3 = 1/[(1 - \frac{1}{\delta_2})(\frac{\lambda_1 P_S}{\lambda_{11} P_{U_1}} - \frac{1}{\delta_2})]$. Making the use of [28, Eq. (3.352.4)], the following proposition is obtained.

Proposition 1. *Exact closed-form expressions for the EC of U_1 can be formulated as*

$$EC_{U_1} = -\frac{\lambda_1 P_S \delta_1/\delta_2}{\ln(2)\lambda_{11} P_{U_1}} \left[\frac{\alpha_1 Ei\left(-\frac{\sigma}{\lambda_1 P_S}\right)}{\exp\left(-\frac{\sigma}{\lambda_1 P_S}\right)} + \frac{\alpha_2 Ei\left(-\frac{\sigma}{\lambda_{11} P_{U_1}}\right)}{\exp\left(-\frac{\sigma}{\lambda_{11} P_{U_1}}\right)} + \frac{\alpha_3 Ei\left(-\frac{\sigma/\delta_2}{\lambda_1 P_S}\right)}{\exp\left(-\frac{\sigma/\delta_2}{\lambda_1 P_S}\right)} \right], \quad (24)$$

where $Ei(\cdot)$ is the exponential integral function [28, Eq. (8.211)].

2) ERGODIC CAPACITY OF U_2

From definition, the total EC of U_2 with case I can be evaluated by

$$\mathrm{EC}_{U_2}^{I} = \mathrm{E}\{\log_2(1+\gamma^{I}_{U_2\to x_{B_1}})\} + \mathrm{E}\{\log_2(1+\gamma^{I}_{U_2\to x_{B_2}})\} = \int_0^\infty \frac{1 - F_{\gamma^{I}_{U_2\to x_{B_1}}}(x)}{\ln(2)(1+x)}dx + \int_0^\infty \frac{1 - F_{\gamma^{I}_{U_2\to x_{B_2}}}(x)}{\ln(2)(1+x)}dx, \quad (25)$$

where

$$F_{\gamma^{I}_{U_2\to x_{B_1}}}(x) = \Pr[\gamma^{I}_{U_2\to x_{B_1}} < x] = F_{|h_{12}|^2}\left(\frac{x\sigma}{P_{U_1}}\right) = 1 - \exp\left(-\frac{x\sigma}{\lambda_{12} P_{U_1}}\right), \forall x \ge 0, \quad (26)$$

$$F_{\gamma^{I}_{U_2\to x_{B_1}}}(x) = \int_0^\infty F_{\|\mathbf{h}_2\|^2}\left(x\frac{P_{U_1} z + \sigma}{\delta_2 P_S}\right) f_{|h_{12}|^2}(z)dz = 1 - \sum_{k=0}^{K-1}\sum_{l=0}^{k} \frac{\binom{k}{l}\sigma^{k-l} l!}{k!\lambda_{12} P_{U_1} (\lambda_2\delta_2 P_S)^{k-l-1}} \frac{x^k \exp\left(-\frac{\sigma x}{\lambda_2 \delta_2 P_S}\right)}{\left(x + \frac{\lambda_2\delta_2 P_S}{\lambda_{12} P_{U_1}}\right)^{l+1}}. \quad (27)$$

Proposition 2. *Exact closed-form expressions for the EC U_2 with case I can be formulated as*

$$EC^{I}_{U_2} = \Phi_1 + \sum_{k=0}^{K-1}\sum_{l=0}^{k} \frac{\binom{k}{l}\sigma^{k-l} l!}{k!\lambda_{12} P_{U_1} (\lambda_2\delta_2 P_S)^{k-l-1}}\Phi_2, \quad (28)$$

where

$$\Phi_1 = -\frac{Ei\left(-\frac{\sigma/\lambda_{12}}{P_{U_1}}\right)}{\ln(2)\exp\left(-\frac{\sigma/\lambda_{12}}{P_{U_1}}\right)}, \quad (29)$$

$$\Phi_2 = \left(\frac{\lambda_{12} P_{U_1}}{\lambda_2\delta_2 P_S - \lambda_{12} P_{U_1}}\right)^{l+1} \frac{\Gamma(k+1)\Gamma\left(-k, \frac{\sigma/\lambda_2}{\delta_2 P_S}\right)}{\ln(2)\exp\left(-\frac{\sigma/\lambda_2}{\delta_2 P_S}\right)} + \sum_{t=0}^{l} \frac{\Psi^{(t)}\left(-\frac{\lambda_2\delta_2 P_S}{\lambda_{12} P_{U_1}}\right)}{t!\ln(2)} \sum_{m=0}^{k} \frac{\binom{k}{m}\left(-\frac{\lambda_2\delta_2 P_S}{\lambda_{12} P_{U_1}}\right)^{k-m}}{\exp\left(-\frac{\sigma}{\lambda_{12} P_{U_1}}\right)} \frac{\Gamma\left(m+t-l, \frac{\sigma/\lambda_{12}}{P_{U_1}}\right)}{(\sigma/[\lambda_2\delta_2 P_S])^{m+t-l}}. \quad (30)$$

Proof: The proof of the above can be done by two folds: (1) plugging (26) into the first integral in (25) and then invoking [28, Eqs. (3.352.4)] to get Φ_1 in (29); and (2) inserting (27) into the second integral in (25) and then exploiting the partial fraction approach in [7, Eq. (35)] to decompose $1/(1+x)/(x+\lambda_2\delta_2/[\lambda_{12} P_{U_1}])^{l+1}$ as

$$\Phi_2 = \left(\frac{\lambda_{12} P_{U_1}}{\lambda_2\delta_2 P_S - \lambda_{12} P_{U_1}}\right)^{l+1} \int_0^\infty \frac{x^k \exp\left(-\frac{\sigma x}{\lambda_2\delta_2 P_S}\right)dx}{\ln(2)(x+1)} + \sum_{t=0}^{l} \frac{\Psi^{(t)}\left(-\frac{\lambda_2\delta_2 P_S}{\lambda_{12} P_{U_1}}\right)}{t!\ln(2)} \int_0^\infty \frac{x^k \exp\left(-\frac{\sigma x}{\lambda_2\delta_2 P_S}\right)}{\left(x + \frac{\lambda_2\delta_2 P_S}{\lambda_{12} P_{U_1}}\right)^{l+1-t}}dx.$$

Herein, $\Psi(x) = 1/(x+1)$ and $\Psi^{(t)}(x)$ means the t-th order derivative of $\Psi(x)$ with respect to x. Accordingly, the first above is solved using [28, Eq. (3.383.10)] while the second integral is required to first use the transformation $y = x + \lambda_2\delta_2 P_S/[\lambda_{12} P_{U_1}]$, then the binomial theorem for $(y - \lambda_2\delta_2 P_S/[\lambda_{12} P_{U_1}])^k$ and finally, the identity of [28, Eq. (3.381.3)]. Combining all of them, one arrives at the final solution for Φ_2 in (30). ■

Likewise, the total EC of U_2 with case II is expressed as

$$\mathrm{EC}_{U_2}^{II} = \int_0^\infty \frac{1 - F_{\gamma^{II}_{U_2\to x_{B_1}}}(x)}{\ln(2)(1+x)}dx + \int_0^\infty \frac{1 - F_{\gamma^{II}_{U_2\to x_{B_2}}}(x)}{\ln(2)(1+x)}dx, \quad (31)$$

where

$$F_{\gamma^{III}_{U_2\to x_{B_1}}}(x) = \int_0^\infty F_{|h_{12}|^2}\left(x\frac{\delta_2 P_S z + \sigma}{P_{U_1}}\right) f_{\|\mathbf{h}_2\|^2}(z)dz = 1 - \frac{\exp\left(-\frac{\sigma/\lambda_{12}}{P_{U_1}}x\right)}{\left(\frac{\lambda_2\delta_2 P_S}{\lambda_{12} P_{U_1}}\right)^K \left(x + \frac{\lambda_{12} P_{U_1}}{\lambda_2\delta_2 P_S}\right)^K}, \quad (32)$$

$$F_{\gamma^{III}_{U_2\to x_{B_2}}}(x) = F_{\|\mathbf{h}_2\|^2}\left(\frac{x\sigma}{\delta_2 P_S}\right) = 1 - \sum_{k=0}^{K-1} \frac{1}{k!}\left(\frac{\sigma/\lambda_2}{\delta_2 P_S}\right)^k x^k \exp\left(-\frac{\sigma/\lambda_2}{\delta_2 P_S}x\right). \quad (33)$$

Proposition 3. *Exact closed-form expressions for the EC U_2 with case II can be formulated as*

$$EC^{II}_{U_2} = \Phi_3 + \Phi_4, \quad (34)$$

where

$$\Phi_3 = -\left(\frac{\lambda_{12}P_{U_1}}{\lambda_{12}P_{U_1} - \lambda_2\delta_2 P_S}\right)^K \frac{Ei(-\sigma/[\lambda_{12}P_{U_1}])}{\ln(2)\exp(-\sigma/[\lambda_{12}P_{U_1}])} + \sum_{t=0}^{K-1} \frac{\Psi^{(t)}\left(-\frac{\lambda_{12}P_{U_1}}{\lambda_2\delta_2 P_S}\right)\left(-\frac{\sigma}{\lambda_{12}P_{U_1}}\right)^{K-t-1}}{t!\ln(2)\left(\frac{\lambda_2\delta_2 P_S}{\lambda_{12}P_{U_1}}\right)^K (K-t-1)!} \left[\sum_{k=1}^{K-t-1} \frac{(k-1)!}{(-\sigma/[\lambda_2\delta_2 P_S])^k} - \frac{Ei(-\sigma/[\lambda_2\delta_2 P_S])}{\exp(-\sigma/[\lambda_2\delta_2 P_S])}\right], \quad (35)$$

$$\Phi_4 = \sum_{k=0}^{K-1} \frac{1}{k!\ln(2)}\left(\frac{\sigma/\lambda_2}{\delta_2 P_S}\right)^k \left[\sum_{m=1}^{k} \frac{(m-1)!(-1)^{k-m}}{(\sigma/[\lambda_2\delta_2 P_S])^m} - \frac{(-1)^k Ei\left(-\sigma/[\lambda_2\delta_2 P_S]\right)}{\exp\left(-\sigma/[\lambda_2\delta_2 P_S]\right)}\right]. \quad (36)$$

Proof: After substituting (32) into the first integral in (31) and then exploiting the partial fraction approach in [7, Eq. (35)] to decompose $1/(1+x)/(x+\lambda_{12}P_{\mathrm{U}_1}/[\lambda_2\delta_2 P_{\mathrm{S}}])^K$, one has that

$$\Phi_3 = \left(\frac{\lambda_{12}P_{\mathrm{U}_1}}{\lambda_{12}P_{\mathrm{U}_1} - \lambda_2\delta_2 P_{\mathrm{S}}}\right)^K \int_0^\infty \frac{\exp\left(-\frac{x\sigma}{\lambda_{12}P_{\mathrm{U}_1}}\right)dx}{\ln(2)(x+1)} + \sum_{t=0}^{K-1} \frac{\Psi^{(t)}\left(-\frac{\lambda_{12}P_{\mathrm{U}_1}}{\lambda_2\delta_2 P_{\mathrm{S}}}\right)}{t!\ln(2)\left(\frac{\lambda_2\delta_2 P_{\mathrm{S}}}{\lambda_{12}P_{\mathrm{U}_1}}\right)^K} \int_0^\infty \frac{\exp\left(-\frac{x\sigma}{\lambda_{12}P_{\mathrm{U}_1}}\right)dx}{\left(x+\frac{\lambda_{12}P_{\mathrm{U}_1}}{\lambda_2\delta_2 P_{\mathrm{S}}}\right)^{K-t}}.$$

By using the integral above can be solved using [28, Eq. (3.353.2)], and after some algebraic steps, one can attain the final solution for Φ_3 in (35). Meanwhile, after substituting (33) into (31) and then making the use of [28, Eq. (3.353.1)], one achieves the result of Φ_4 in (36). ■

Finally, by performing the analogue as case II, one can attain the following proposition.

Proposition 4. *Exact closed-form expressions for the EC U_2 with case III can be formulated as*

$$EC_{U_2}^{III} = \Phi_4 + \Phi_5, \quad (37)$$

where

$$\Phi_5 = -\left(\frac{\lambda_{12}P_{U_1}}{\lambda_{12}P_{U_1} - \lambda_2 P_S}\right)^K \frac{Ei(-\sigma/[\lambda_{12}P_{U_1}])}{\ln(2)\exp(-\sigma/[\lambda_{12}P_{U_1}])} + \sum_{t=0}^{K-1} \frac{\Psi^{(t)}\left(-\frac{\lambda_{12}P_{U_1}}{\lambda_2 P_S}\right)\left(-\frac{\sigma}{\lambda_{12}P_{U_1}}\right)^{K-t-1}}{t!\ln(2)\left(\frac{\lambda_2 P_S}{\lambda_{12}P_{U_1}}\right)^K (K-t-1)!} \left[\sum_{k=1}^{K-t-1} \frac{(k-1)!}{(-\sigma/[\lambda_2 P_S])^k} - \frac{Ei(-\sigma/[\lambda_2 P_S])}{\exp(-\sigma/[\lambda_2 P_S])}\right]. \quad (38)$$

IV. NUMERICAL RESULTS

This section presents simulated results to corroborate the theoretical analysis and evaluate the performances of the considered systems. All the simulated outcomes are obtained using Monte-Carlo approaches with 10^4 channel realizations. Considering the impact of pathloss propagation, the scale parameters of channels are modeled as $\lambda_1 = \mathtt{L}d_1^{-\mathtt{path}}$, $\lambda_2 = \mathtt{L}d_2^{-\mathtt{path}}$, $\lambda_{12} = \mathtt{L}d_{12}^{-\mathtt{path}}$, and $\lambda_{11} = -30$ dB, where $\mathtt{L} = 30$ dB is the attenuation transmitted power at the unit reference distance (1 m) and $\mathtt{path} = 2.7$ is the pathloss exponent while $d_1 = 10$ m, $d_2 = 20$, and $d_{12} = 10$ corresponds to the physical distance of S-U_1, S-U_2, and U_1-U_2, respectively.

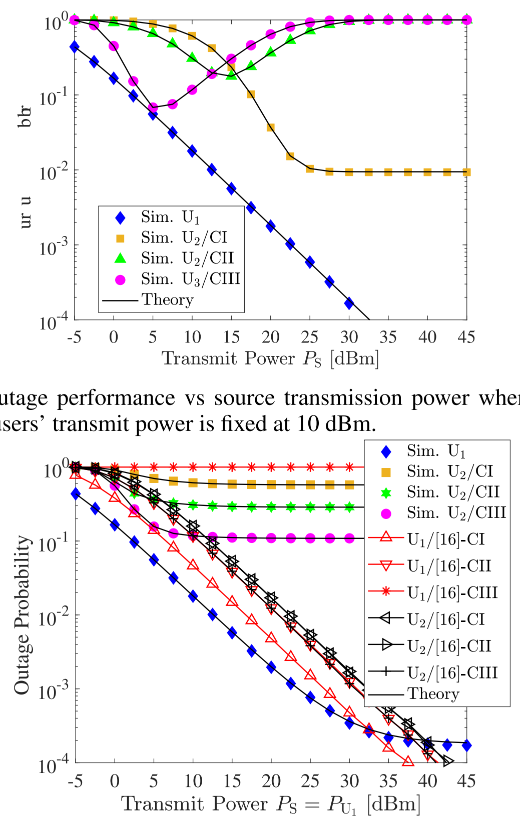

(a) Outage performance vs source transmission power when near ship users' transmit power is fixed at 10 dBm.

(b) Outage performance vs the equivalent transmission power between source and near ship users.

FIGURE 2. Effect of transmit power on the users' OP with the fixed system parameters: $\sigma = 1$, $\delta_1 = 0.6$, $K = 4$, $R_A = 0.25$ bit/s/Hz, $R_{B_2} = 0.5$ bit/s/Hz, and $R_{B_1} = 0.25$ bit/s/Hz.

A. OUTAGE PROBABILITY EVALUATION

Fig. 2 illustrates the effect of the transmission power on the users' outage performance. The markers indicate the simulated outcome (i.e., sim), while the solid line plots represent the theory results brought by Lemmas 1-4. In the legend of the figure, CI, CII, and CIII are the labels of cases I, II, and III, respectively. As illustrated in Fig. 2, the developed theories are in excellent agreement with the simulation results. Next, it is observed in Fig. 2a that when $P_{\mathrm{S}} \gg P_{\mathrm{U}_1}$, the OP of U_1 improves significantly, and it tends to converge to zero. The OP of U_2 with case I becomes saturated, whereas those of U_2 with cases II and III increase, and they are in outage as P_{S} exceeds 30 dBm. However, for

$P_S \ll P_{U_1}$, the OP of users are almost converged to 1. On the other hand, it can be also seen from Fig. 2b that all users' OP are saturated as $P_S \approx P_{U_1}$. Clearly, these observations are well fit with what is deduced after each developed Lemma. Moreover, Fig. 2a also remarkably shows an interesting observation in choosing the decoding order at U_2. Specifically, U_2 is preferable to use the decoding order of case III when P_S is set to be lower than P_{U_1}. Otherwise, the decoding order of case I should be adopted. Notably, there is an optimal source transmission power when $P_S \leq P_{U_1}$, at which the OP of U_2 is minimized. Meanwhile, the result in Fig. 2b confirms that the OP of U_2 is only improved with the decoding order of case III while its performance is decreased with the decoding order of case I. In comparison with the scheme developed in [16], our proposed scheme shows superior OP performance for U_1 from -5 dBm to 40 dBm. This is because U_1 only carries out one decoding process for its message, while that of U_1 (relay nodes) in [16] requires SIC for two processing signals of itself and U_2 (destination nodes). On the other hand, it is shown that the OP of the proposed scheme has less performance than that of U_2 in [16] at moderate and high transmit power regimes. This is because in [16], U_1 performs cooperative communication by means of forwarding the decoded signal in the first phase to enhance the quality of U_2 in the second phase, at which U_2 exploits maximal-ratio combining approach to boost its decoding ability. Meanwhile, our scheme focuses on sending cached signals aiming to enhance the spectral efficiency for U_2. Thus, exploiting the SIC process at U_2 increases the OP for U_2. However, it should be noted that the superiority of spectral efficiency (known as ergodic capacity) will be soon discussed in the following figure.

Fig. 3 represents the user's OP when the number of antenna settings increases. Since the designed beamforming only aims to improve the performance of U_2, the increased number of antennas installed at the base station does not play any role in enhancing U_1' performance, leading to the OP constant of U_1. While for U_2, the increased number of antennas shows some different trends with distinct transmit power settings. In Fig. 3a, while the OP with cases I and II linearly decreases with the increment of K, that of cases III increases. The reason for the former phenomenon is that increasing the number of antennas helps U_2 to have more chances to boost the decoding ability: case I with higher successful decoding probability for x_A and x_{B_2} and case II with higher successful decoding probability for x_{B_2}. Meanwhile, the reason for the latter phenomenon is that the increased number of antennas increases interference noise in decoding x_{B_1}, yielding an overall OP degradation. In Fig. 3b, when K increases, the OP of U_2 with the case I obtains first improves, and its trends then become saturated. Inversely, the OPs of U_2 with cases II and III are increased due to the increment of inference in decoding x_{B_1}. In Fig. 3c, when K is in the low regime, the decoding order with case III yields the best OP improvement. When K is in the moderate regime, the decoding order with case II shows its best performance. However, in a high

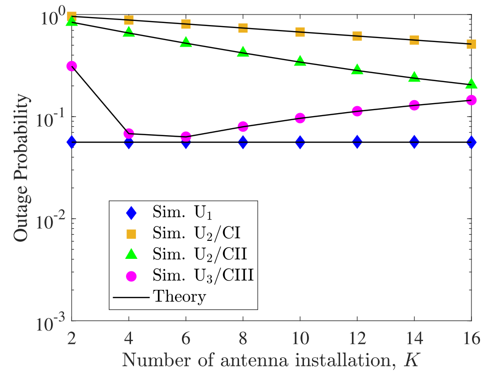

(a) $P_S \ll P_{U_1}$: $P_S = 5$ dBm and $P_{U_1} = 10$ dBm.

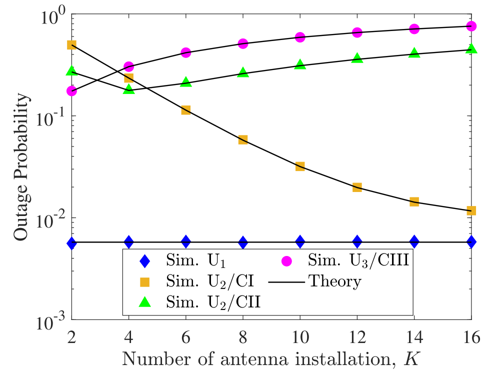

(b) $P_S \gg P_{U_1}$: $P_S = 15$ dBm and $P_{U_1} = 10$ dBm.

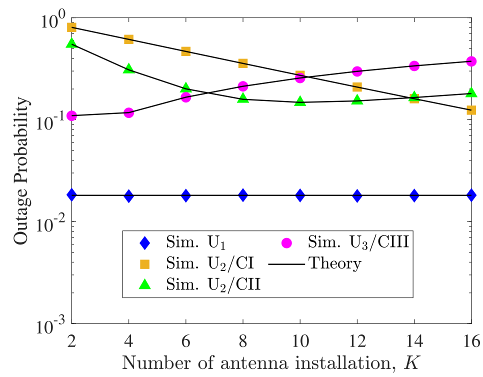

(c) $P_S \approx P_{U_1}$: $P_S = P_{U_1} = 10$ dBm.

FIGURE 3. Effect of the number of antenna settings on the users' OP.

number of antenna setting regimes, the OP of U_2 is only improved when the decoding order follows case III.

Fig. 4 illustrates how the PA factor dictates the users' OP. As the PA factor δ_1 increases, the more power budget is allocated to the information signal x_A, thereby decreasing the OP of U_1. In contrast, the OP of U_2 varies with different decoding orders as well as the relation between P_S and P_{U_1}. In Fig. 4a, the realization of case III can offer the best OP improvement for U_2, and especially the OP of U_2 can be further improved by optimizing the PA coefficient δ_1 that can be readily achieved using some one dimension search approaches with low computational complexity, viz., bisection search or golden search. In Fig. 4b, it is found that when δ_1 varies from 0.3 to 0.5, the OP of U_2 obtains the best improvement with case I. However, when δ_1 is belong to (0.5, 1), it is recommended to use the decoding order involving the case II to get in touch with the best OP improvement for U_2. Besides, the result also shed light on the fact that allowing $\delta_1 \in (0.6, 1)$ is also a reasonable solution as it can simultaneously achieve the OP improvement for U_1. In Fig. 4c, it can be seen that the performance of U_2 has the similar trend as in Fig. 4c, where the OP of U_2 can be only improved with case III.

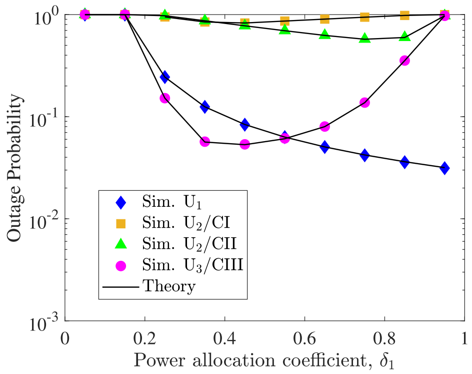

(a) $P_S \ll P_{U_1}$: $P_S = 5$ dBm and $P_{U_1} = 10$ dBm.

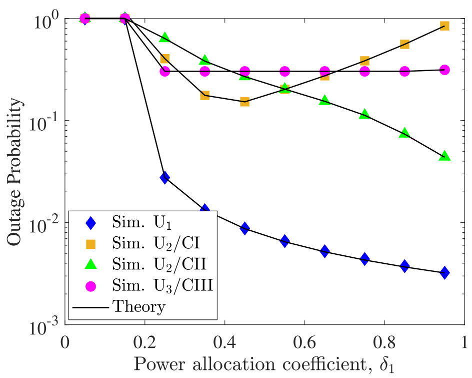

(b) $P_S \gg P_{U_1}$: $P_S = 15$ dBm and $P_{U_1} = 10$ dBm.

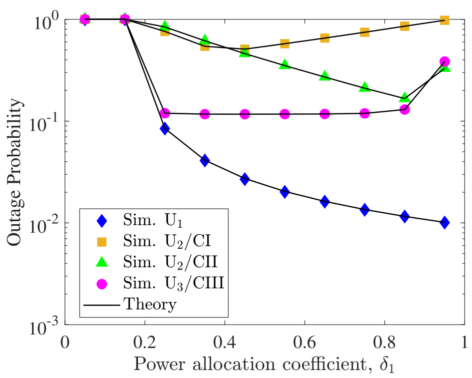

(c) $P_S \approx P_{U_1}$: $P_S = P_{U_1} = 10$ dBm.

FIGURE 4. Effect of the PA factor on the users' OP.

B. ERGODIC CAPACITY EVALUATION

Fig. 5 represents the EC for users under distinct power settings. It is observed from the figure that the proposed

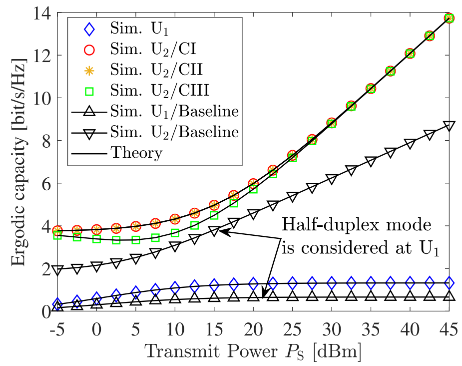

(a) EC performance vs source transmission power when near ship users' transmit power is fixed at 10 dBm.

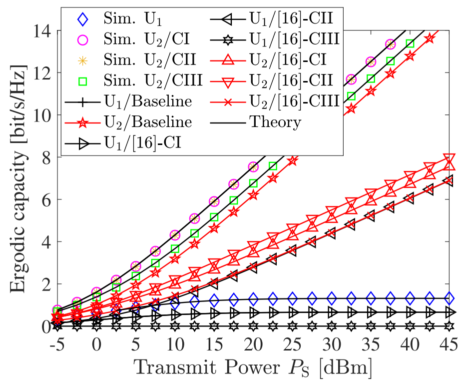

(b) EC performance vs the equivalent transmission power between source and near ship users, $P_S \approx P_{U_1}$.

FIGURE 5. Effect of transmit power on the users' EC with the fixed system parameters: $\sigma = 1$, $\delta_1 = 0.6$, and $K = 4$.

system achieves outstanding EC enhancement compared to that of half-duplex D2D communications (i.e., baseline), irrespective of how the power-setting scenario is. For the EC of U_1, it is clear that the EC produced by the proposed system is twice that of the baseline. This is because the former can fully use transmission time to convey information to users, while the latter only exploits half of the duration period. For the EC of U_2, it is found that U_2 with three proposed decoding order schemes always achieves a higher EC improvement compared to the EC produced by the baseline. In addition, when P_S increases, the EC produced by cases I and II is almost the same even though there is an OP discrepancy, as discussed in Figs. 2-4. This phenomenon can be readily justified by mathematically using the fact that $\log(1 + x/y) = \log(x + y) - \log(x)$ when evaluating the EC for these cases. However, there are two remarkable EC trends among Fig. 5a and Fig. 5b. First, U_2 with case III in Fig. 5a has the lowest EC performance at low and moderate P_S regimes, while in Fig. 5b, increasing in parallel. Second, as P_S increases, the EC gap produced by the three cases proposed in Fig. 5 improves significantly, whereas those of Fig. 5b keep the same. However, there is a key point: the adoption of cases I and II gain 5 dB of transmit power saving

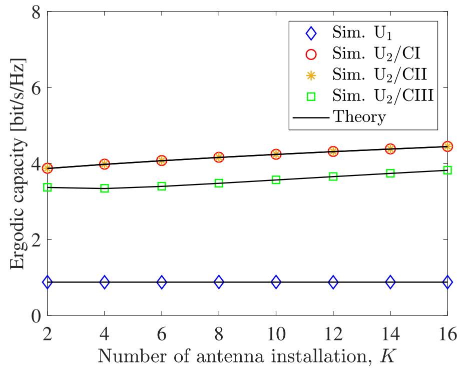

(a) $P_S \ll P_{U_1}$: $P_S = 5$ dBm and $P_{U_1} = 10$ dBm.

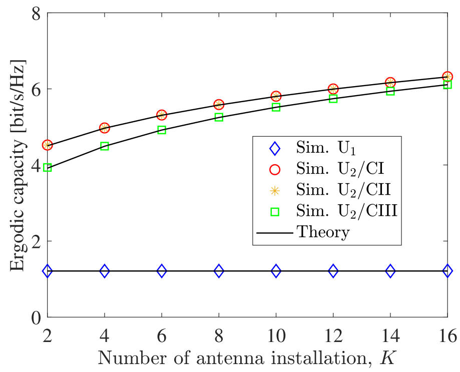

(b) $P_S \gg P_{U_1}$: $P_S = 15$ dBm and $P_{U_1} = 10$ dBm.

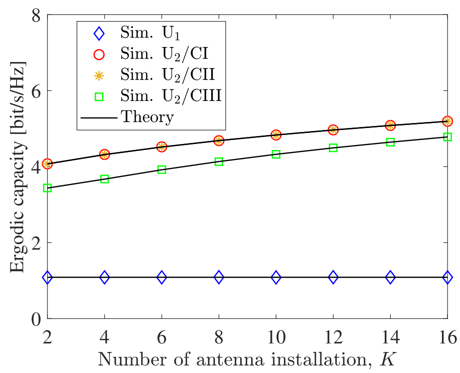

(c) $P_S \approx P_{U_1}$: $P_S = P_{U_1} = 10$ dBm.

FIGURE 6. Effect of the number of antenna settings on the users' EC.

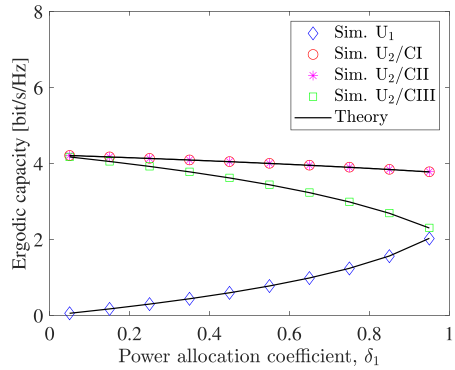

(a) $P_S \ll P_{U_1}$: $P_S = 5$ dBm and $P_{U_1} = 10$ dBm.

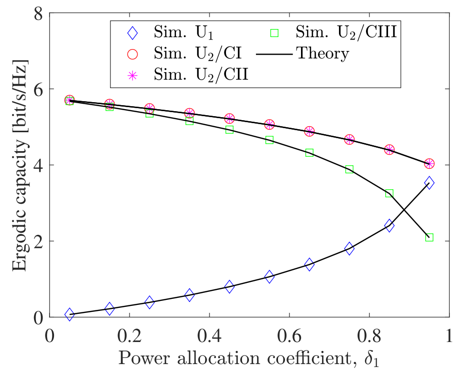

(b) $P_S \gg P_{U_1}$: $P_S = 15$ dBm and $P_{U_1} = 10$ dBm.

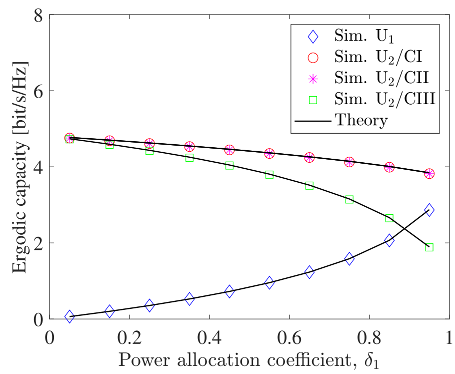

(c) $P_S \approx P_{U_1}$: $P_S = P_{U_1} = 10$ dBm.

FIGURE 7. Effect of PA coefficient δ_1 on the users' EC.

when compared to the baseline, while for case III, 2.5 dB. On another front, it is observed from Fig. 5b that U_2 in our proposed scheme shows superior ergodic capacity compared to U_2 in [16]. This exactly agrees with our mentioned in the discussion of Fig. 5b, leveraging caching solution enables U_2 to double chances to enhance its spectral efficiency, one from the coastal base station and the other from U_1-aided communication. Besides, the figure also shows that the EC of U_1 outperforms those of cases I and III in [16] although there is an EC degradation in our proposed scheme compared to that of [16]. This is due to the fact that on the one hand, the system in [16] operates in half-duplex mode, leading to the capacity of U_1 for case I reduce a half compared to the EC of U_1 in our proposed scheme. On the other hand, for case III, U_1 fails to decode its signals, leading to zero-ergodic capacity. In this case, there is no cooperative communication between U_1 and U_2. Regarding case II, U_1 in [16] exploits SIC to mitigate inter-user interference from its reception signal, giving rise to the EC improvement. However, it is worth noting that taking into account the sum ergodic rate perspective, our proposed schemes are still promising as we can allocate more power to U_1 while exploiting multi-antenna transmission to boost the EC of U_2 or choosing the scheme with fewer effects of power allocation issues, thereby

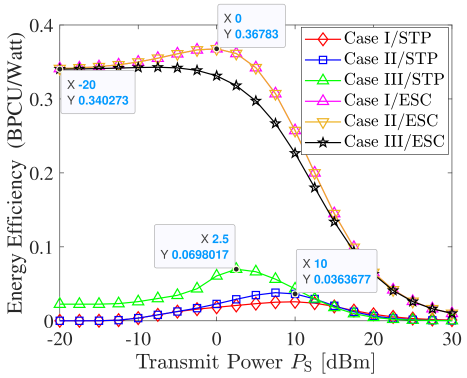

(a) Energy efficiency vs source transmission power when near ship users' transmit power is fixed at 10 dBm.

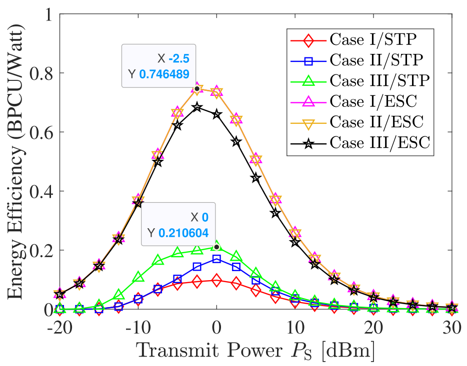

(b) Energy efficiency vs the equivalent transmission power between source and near ship users, $P_S \approx P_{U_1}$.

FIGURE 8. Energy efficiency vs the transmit power. Setups: $\sigma = 1$, $\delta_1 = 0.6$, and $K = 4$.

choosing the right power budget for U_1 to speed up its EC. Note that such features cannot be obtained in [16] due to only a single antenna at the base station. Details of multi-antenna transmission as well as power distribution issues will be presented in the following figures.

Figs. 6 and Fig. 7 explore the users' EC behavior under a different number of antennas installed at the base station and the PA design. As depicted in Fig. 6, the EC of U_1 has no change with the increase of K due to the same reason as clarified in Fig. 3. Meanwhile, the EC of U_2 tends to slightly increase as K increases, and it obtains the best improvement as $P_S \gg P_{U_1}$. It is because the design of the beamforming vector and the corresponding power signal strength are jointly boosted. In Fig. 7, there is a EC trade-off in power budget allocation. Specifically, as δ_1 increases, the EC of U_1 is improved due to more power allocated to its signal. Inversely, the EC of U_2 decreases as δ_1 increases. This is because of a decrease in the power budget allocated to the signal of B_2. Similar to Fig. 6, as $P_S \gg P_{U_1}$, the user EC improves.

Fig. 8 shows the average energy efficiency (EE) as a function of the transmit power under two cases: 1) sum throughput (STP) and 2) ergodic sum capacity (ESC). The function EE herein is determined by the ratio between STP and the total transmit power ($P_S + P_{U_1}$) plus circuit consumption ($P_{\text{circuit}} = 1$ watt) [4]. As we can see, in Fig. 8(a), the EE curves of ESC with cases I and II tend to increase from $P_S = -20$ dBm to $P_S = 0$ dBm, reaching out the maximum value at $P_S = 0$, and then rapidly reduce to zero with high transmit power regime. Meanwhile, the EE curve of ESC with case III maintains the maximum value when P_S varies from -20 dBm to -5 dBm and then decreases to zero as $P_S = 0$ increases. On the other hand, one can observe that all of the EE curves of ESC have a concave form, where the EE curve of STP with case III reaches its maximum value at $P_S = 0$, while those of STP with cases I and II show their maximum values at $P_S = 10$ dBm. Unlike Fig. 8(a), all the EE curves in Fig. 8(b) show a concave form, where the EE curves of ESC have the maximum value at $P_S = -2.5$ dBm, while those of STP maximization is when $P_S = 0$ dBm. The reason for these observations is that when P_S is large, the circuit's power consumption dominates, which has a negative impact on EE performance. On the other hand, it is also observed from Fig. 8 that the EE produced by adopting $P_S \approx P_{U_1}$ yields better performance than that of fixed P_{U_1}. The reason is that increasing P_{U_1} offers a better-enhanced performance for D2D communication between the near and far users, leading to higher STP and ESC improvement.

V. CONCLUSION

This work has investigated the performance of NOMA with cache-aided maritime full-duplex D2D communication networks, where a joint PA policy and beamforming design is considered to meet the quality of service for near-ship users while also enhancing the performance of far-ship users. Moreover, three decoding order schemes aware of the D2D communication were also presented and quantified to provide a comprehensive observation in improving the performance of far ship users. Exact closed-form expressions for the users' OP and EC were derived, and from which guidelines some useful insight related to the trade-off between the base station and the D2D transmission powers. Numerical results validated our analysis and showed the superiority of the proposed system with three decoding order schemes in terms of EC when compared to NOMA ache-aided maritime half-duplex D2D networks and conventional cooperative NOMA communication. Besides, there was a slight outage performance degradation for far ship users; however, such a problem could be tackled via the right chosen decoding order scheme, proper power allocation alignments or increasing the number of antenna transmissions.

Although this work delivered a potential solution to enhance the performance of far ships users by means of proposing three decoding orders, the research on caching-aided communication has some limitations, such as dynamic cooperative communications, imperfect channel state estimations or hardware impairment issues. These are promising research directions that need to be further addressed for future practical implementations.

REFERENCES

[1] L. Dai, B. Wang, Y. Yuan, S. Han, I. Chih-lin, and Z. Wang, ''Non-orthogonal multiple access for 5G: Solutions, challenges, opportunities, and future research trends,'' *IEEE Commun. Mag.*, vol. 53, no. 9, pp. 74–81, Sep. 2015.

[2] T. Yoon, T. H. Nguyen, X. T. Nguyen, D. Yoo, B. Jang, and V. D. Nguyen, ''Resource allocation for NOMA-based D2D systems coexisting with cellular networks,'' *IEEE Access*, vol. 6, pp. 66293–66304, 2018.

[3] T.-T. Nguyen, T.-H. Vu, T.-V. Nguyen, D. B. D. Costa, and C. D. Ho, ''Underlay cognitive NOMA-based coordinated direct and relay transmission,'' *IEEE Wireless Commun. Lett.*, vol. 10, no. 4, pp. 854–858, Apr. 2021.

[4] T.-H. Vu, T.-V. Nguyen, and S. Kim, ''Cooperative NOMA-enabled SWIPT IoT networks with imperfect SIC: Performance analysis and deep learning evaluation,'' *IEEE Internet Things J.*, vol. 9, no. 3, pp. 2253–2266, Feb. 2022.

[5] M. Le-Tran, T.-H. Vu, and S. Kim, ''Performance analysis of optical backhauled cooperative NOMA visible light communication,'' *IEEE Trans. Veh. Technol.*, vol. 70, no. 12, pp. 12932–12945, Dec. 2021.

[6] T.-H. Vu, T.-V. Nguyen, D. B. D. Costa, and S. Kim, ''Reconfigurable intelligent surface-aided cognitive NOMA networks: Performance analysis and deep learning evaluation,'' *IEEE Trans. Wireless Commun.*, vol. 21, no. 12, pp. 10662–10677, Dec. 2022.

[7] T.-H. Vu, T.-V. Nguyen, Q.-V. Pham, D. B. D. Costa, and S. Kim, ''Hybrid long- and short-packet based NOMA systems with joint power allocation and beamforming design,'' *IEEE Trans. Veh. Technol.*, vol. 72, no. 3, pp. 4079–4084, Mar. 2023.

[8] V. S. Nguyen and T. H. Nguyen, ''Performance analysis of cognitive-inspired wireless powered NOMA systems with joint collaboration,'' *IEEE Access*, vol. 11, pp. 51578–51589, 2023.

[9] Y. Xu, J. Tang, B. Li, N. Zhao, D. Niyato, and K.-K. Wong, ''Adaptive aggregate transmission for device-to-multi-device aided cooperative NOMA networks,'' *IEEE J. Sel. Areas Commun.*, vol. 40, no. 4, pp. 1355–1370, Apr. 2022.

[10] K. Z. Shen, D. K. C. So, J. Tang, and Z. Ding, ''Power allocation for NOMA with cache-aided D2D communication,'' *IEEE Trans. Wireless Commun.*, early access, May 30, 2023, doi: 10.1109/TWC.2023.3279266.

[11] M. S. M. Gismalla, A. I. Azmi, M. R. B. Salim, M. F. L. Abdullah, F. Iqbal, W. A. Mabrouk, M. B. Othman, A. Y. I. Ashyap, and A. S. M. Supa'at, ''Survey on device to device (D2D) communication for 5GB/6G networks: Concept, applications, challenges, and future directions,'' *IEEE Access*, vol. 10, pp. 30792–30821, 2022.

[12] A. M. H. Alibraheemi, M. N. Hindia, K. Dimyati, T. F. T. M. N. Izam, J. Yahaya, F. Qamar, and Z. H. Abdullah, ''A survey of resource management in D2D communication for B5G networks,'' *IEEE Access*, vol. 11, pp. 7892–7923, 2023.

[13] Y. Fu, Y. Zhang, Q. Zhu, H.-N. Dai, M. Li, and T. Q. S. Quek, ''A new vision of wireless edge caching networks (WECNs): Issues, technologies, and open research trends,'' *IEEE Netw.*, early access, Mar. 13, 2023, doi: 10.1109/MNET.124.2200003.

[14] F. S. Alqurashi, A. Trichili, N. Saeed, B. S. Ooi, and M.-S. Alouini, ''Maritime communications: A survey on enabling technologies, opportunities, and challenges,'' *IEEE Internet Things J.*, vol. 10, no. 4, pp. 3525–3547, Feb. 2023.

[15] Y.-L. Foo, ''Operating white space devices in the DTV service area,'' *ICT Exp.*, vol. 6, no. 1, pp. 7–10, Mar. 2020.

[16] Y. Ji, X. Zhang, G. Zhang, X. Zhu, Q. Sun, and W. Duan, ''Use of NOMA for maritime communication networks with P-DF relaying channel,'' *China Commun.*, vol. 17, no. 7, pp. 236–246, Jul. 2020.

[17] R. Tang, W. Feng, Y. Chen, and N. Ge, ''NOMA-based UAV communications for maritime coverage enhancement,'' *China Commun.*, vol. 18, no. 4, pp. 230–243, Apr. 2021.

[18] C. Jiang, Y. Fu, C. Jiang, and L. Yin, ''Shipping lane-aware caching and transmission scheme for maritime wireless networks,'' in *Proc. Int. Wireless Commun. Mobile Comput. (IWCMC)*, Jun. 2020, pp. 257–262.

[19] H. Feng, Z. Cui, and T. Yang, ''Cache optimization strategy for mobile edge computing in maritime IoT,'' in *Proc. 5th Conf. Cloud Internet Things (CIoT)*, Mar. 2022, pp. 213–219.

[20] J. Zeng, J. Sun, B. Wu, and X. Su, ''Mobile edge communications, computing, and caching (MEC3) technology in the maritime communication network,'' *China Commun.*, vol. 17, no. 5, pp. 223–234, May 2020.

[21] N. Nomikos, P. K. Gkonis, P. S. Bithas, and P. Trakadas, ''A survey on UAV-aided maritime communications: Deployment considerations, applications, and future challenges,'' *IEEE Open J. Commun. Soc.*, vol. 4, pp. 56–78, 2023.

[22] N. Nomikos, A. Giannopoulos, P. Trakadas, and G. K. Karagiannidis, ''Uplink NOMA for UAV-aided maritime Internet-of-Things,'' in *Proc. 19th Int. Conf. Design Reliable Commun. Netw. (DRCN)*, Apr. 2023, pp. 1–6.

[23] X. Fang, W. Feng, Y. Wang, Y. Chen, N. Ge, Z. Ding, and H. Zhu, ''NOMA-based hybrid satellite-UAV-terrestrial networks for 6G maritime coverage,'' *IEEE Trans. Wireless Commun.*, vol. 22, no. 1, pp. 138–152, Jan. 2023.

[24] G. Yu and J. Wu, ''Content caching based on mobility prediction and joint user prefetch in mobile edge networks,'' *Peer-to-Peer Netw. Appl.*, vol. 13, no. 5, pp. 1839–1852, Sep. 2020.

[25] A. Sidiropoulos, G. Pallis, D. Katsaros, K. Stamos, A. Vakali, and Y. Manolopoulos, ''Prefetching in content distribution networks via web communities identification and outsourcing,'' *World Wide Web*, vol. 11, no. 1, pp. 39–70, Mar. 2008.

[26] M. Vaezi, R. Schober, Z. Ding, and H. V. Poor, ''Non-orthogonal multiple access: Common myths and critical questions,'' *IEEE Wireless Commun.*, vol. 26, no. 5, pp. 174–180, Oct. 2019.

[27] T.-H. Vu and S. Kim, ''Performance analysis of full-duplex two-way RIS-based systems with imperfect CSI and discrete phase-shift design,'' *IEEE Commun. Lett.*, vol. 27, no. 2, pp. 512–516, Feb. 2023.

[28] A. Jeffrey and D. Zwillinger, *Table of Integrals, Series, and Products*. Amsterdam, The Netherlands: Elsevier, 2007.

TIEN HOA NGUYEN (Member, IEEE) received the Dipl.-Ing. degree in electronics and communication engineering from Hanover University, Germany. He was with the Research and Development Department of image processing and in the development of SDR-based drivers in Bosch, Germany. He devoted three years of experimentation with MIMOon's Research and Development Team to develop embedded signal processing and radio modules for LTE-A/4G. He was a Senior Expert with the Viettel IC Design Center (VIC) and VinSmart for development of advanced solutions for aggregating and splitting/steering traffic at the PDCP layer and above, to provide robust and QoS/QoE guaranteeing integration between heterogeneous link types in 5G systems. Currently, he is a Lecturer with the School of Electrical and Electronic Engineering, Hanoi University of Science and Technology. His research interests include resource allocation in B5G/6G, massive MIMO, and vehicular communication systems.

JOOPYOUNG CHOI was born in Seoul, South Korea, in April 1975. He received the M.S. degree in electronic engineering, in 2001, and the Ph.D. degree in information and telecommunication engineering from Soongsil University, Seoul, in 2010. He is currently a Chief Executive Officer with Institute for Spectrum Insight Company Ltd., Cheongju. His research interests include spectrum sharing policy and technology, cognitive radio, and radio compatibility and interference analysis and antenna array signal processing.

SEONGGYOON PARK received the B.S. degree in electronic engineering, in 1985, the M.S. degree in electronic engineering, in 1987, and the Ph.D. degree in electronic engineering from Yonsei University, Seoul, South Korea, in 1994. He is currently a Professor with the Radio Engineering Department, Information & Communication School, Kongju National University, Cheonan, South Korea. His research interests include 5G and wireless communications technology, radio compatibility and interference analysis, and public safety communications.

BU-YOUNG KIM received the B.S. and M.S. degrees from the School of Navigation, Korea Maritime & Ocean University, Busan, Republic of Korea, in 2004 and 2010, respectively. He is currently a Senior Engineer with the Ocean and Maritime Digital Technology Research Division, Korea Research Institute of Ships & Ocean Engineering, Republic of Korea. He has been researching about developing technology of maritime safety and communication, since 2010, in Korea Maritime Transportation Safety Authority (KMTSA) and Korea Research Institute of Ships and Ocean Engineering (KRISO). His research interests include developing technologies of communication and service for implementation of maritime autonomous surface ship.

WOO-SEONG SHIM received the B.S and Ph.D. degrees from the School of Electronic Engineering, Chungnam National University, Daejeon, Republic of Korea, in 1997 and 2017, respectively. He is currently a Principal Researcher in maritime safety research by ICT technology with the Korea Research Institute of Ships & Ocean Engineering, Republic of Korea. In his 24 years career, including the technical surveyor of ship electrical engineering with Korean Register, from 2005 to 2011, he has focused on developing maritime ICT systems, such as ECDIS with ENC development, AIS, and communication infrastructure for e-navigation. He was the project manager of LTE-maritime to develop the world-first high-speed maritime communication based on LTE technology on the coastal water of South Korea within 100km in maximum. His research interests include developing a high-bandwidth maritime mobile service to provide enough communication channels for maritime use cases, such as e-navigation implementation and the ship-to-ship channel of the maritime autonomous surface ship in the remit of on-going research project.